energies

MDPI

Article

Additional Compound Damping Control to Suppress Low-Frequency Oscillations in a Photovoltaic Plant with a Hybrid Energy Storage System

Kanglin Dai [1], Wei Xiong [1,*], Xufeng Yuan [1,*], Huajun Zheng [1], Qihui Feng [2], Yutao Xu [2], Yongxiang Cai [2] and Dan Guo [1]

[1] College of Electrical Engineering, Guizhou University, Guiyang 550025, China
[2] Electric Power Research Institute of Guizhou Power Grid Co., Ltd., Guiyang 550002, China
* Correspondence: wxiong@gzu.edu.cn (W.X.); xfyuan@gzu.edu.cn (X.Y.)

Abstract: The use of the conventional dual closed-loop control strategy by photovoltaic (PV) plants with grid-connected inverters may weaken the damping of a power system, which may aggravate low-frequency oscillations (LFOs). This influence will become more severe as the penetration of PV plants increases. Therefore, it is necessary to incorporate damping controls into PV plants to suppress LFOs. This paper proposed an additional compound damping control (ACDC) system that combines additional damping control (ADC) for the inverter with ADC-based dynamic power compensation control (DPCC), allowing hybrid energy storage systems (HESSs) to suppress LFOs. First, the feasibility of suppressing low-frequency oscillations in PV plants is demonstrated by the torque method and a small signal model. Then, an additional damping controller is added to the active power control link of the PV inverter to enhance the damping abilities of the system. However, given that the damping performance of PV plants with only ADC is limited by the compensated power, PV plants require devices that can rapidly compensate for the damping power. Therefore, we added the HESS to the DC bus and proposed DPCC. Finally, a three-machine nine-node system for a PV plant was modeled and simulated in the PSCAD platform. The simulation results showed that the proposed control strategy could provide effective damping for interarea oscillation.

Keywords: photovoltaic plant; low-frequency oscillation; additional damping control; dynamic power compensation control; hybrid energy storage system

Citation: Dai, K.; Xiong, W.; Yuan, X.; Zheng, H.; Feng, Q.; Xu, Y.; Cai, Y.; Guo, D. Additional Compound Damping Control to Suppress Low-Frequency Oscillations in a Photovoltaic Plant with a Hybrid Energy Storage System. *Energies* **2022**, *15*, 9044. https://doi.org/10.3390/en15239044

Academic Editor: Enrique Romero-Cadaval

Received: 9 October 2022
Accepted: 23 November 2022
Published: 29 November 2022

1. Introduction

Globally, due to the rapid consumption of fossil fuels and the continuous deterioration of the environment, renewable and clean energy sources have become a research focus. These include energies such as wind and solar energy. Wind and solar energy are expected to meet 50% of the global energy demand by 2050 [1]. Photovoltaic generation systems have been developed especially rapidly, and the installation of large-scale photovoltaic plants is increasing in scale year by year [2]. PV plants differ from traditional power plants and are classified as inverter-based power plants (IBPP) [3]. Since PV plants have no rotating mechanical components, they have no inherent inertia, which increases the risk of LFOs [4]. Low-frequency oscillations can be triggered by a lack of damping or by the system being in a negative damping state, which can cause new electromechanical oscillation modes in severe cases [5,6]. These LFOs are in the frequency range between 0.1 and 2 Hz [7]: the frequency range is 0.1–0.7 Hz for interarea oscillations and 0.7–2 Hz for local oscillations [8]. The problem of how to reduce the interarea oscillations caused by large-scale PV plants has attracted widespread attention.

The most common method for suppressing LFOs in power systems is to install a power system stabilizer (PSS) in the generator, which can offset the negative damping torque generated by the automatic voltage regulator (AVR) and enhance the system's damping

performance [9,10]. PSSs are mainly used to suppress local oscillations, and they are not effective for interarea oscillations [11]. In PV plants, the damping is mainly controlled by altering the power flow of the system, and the lack of a damping control link may have a negative impact on the damping of a system [12]. Adjusting the power output of a PV plant can indirectly change the electromagnetic power of the generator, which enables the PV plant to provide a damping torque to the generator that is sometimes positive and sometimes negative [13–15]. The production of positive damping torque by PV plants is the key to enhancing the oscillation damping of the power system [16]. The location of PV plants can have either positive or negative effects on the low-frequency oscillations [17]. However, PV plants are positioned according to geographic factors and cannot be placed in ideal locations that have little effect on the LFOs; thus, it is essential to design damping controllers for PV plants.

In recent years, wide-area damping control (WADC) has been extensively used to suppress interarea LFOs. In [11], several practical problems and design methods related to WADC are described. In order to reduce the risk posed by the increasing penetration level of PV plants, some PV plants suppress LFOs through power oscillation damping controllers (PODCs) [18]. An optimal damping controller (ODC) was proposed in [19], and the particle swarm optimization (PSO) algorithm was used to determine the controller parameters in order to maximize the damping performance during low-frequency oscillation. The controller mentioned above can be regarded as having the structure of a PSS, which is widely used because of its easy adjustability.

In this paper, an additional damping controller consisting of gain, filter, and phase compensation was used to suppress low-frequency oscillations by combining it with the active reference of the PV inverter. The damping performance of the ADC depends on whether the damping power can be compensated for quickly. To avoid wasting solar energy, PV plants working at the maximum power point at all times cannot provide quick and sufficient power compensation. When there is a margin for PV power output, the margin can compensate for the damping power, and the damping performance depends on the magnitude of the margin at this time. However, the greater the margin, the more solar energy is wasted. Therefore, this paper proposes an additional compound damping control system combining ADC for the inverter and ADC-based DPCC for the HESS to suppress LFOs, with the required damping power of the inverter being provided by the HESS.

The rest of this paper is organized as follows. Section 2 establishes the mathematical model of the SG and analyzes the damping performance of a single-machine infinite-bus system for a PV plant by the torque method. Section 3 demonstrates the feasibility of ADC for the inverter using a small signal model. Section 4 proposes the DPCC system for the HESS. Sections 5 and 6 present the simulation verification and the conclusions, respectively.

2. Single-Machine Infinite-Bus System for a PV Plant

The structure of the single-machine infinite-bus system for a PV plant is shown in Figure 1. The synchronous generator (SG) is connected to the infinite bus through a transmission line with the PV plant. Meanwhile, the PV arrays and the hybrid energy storage system are connected to the inverter through the DC bus. The hybrid energy storage system consists of a super capacitor and a battery, which are safer and more efficient because they only need to perform the functions for which they are suitable. $E_q{}'$ is the transient electromotive force of the q-axis of the synchronous generator. U_v is the bus voltage of the grid-connection point of the PV plant. U_s is the infinite-bus voltage. δ is the phase-angle difference between $E_q{}'$ and U_s. θ is the phase-angle difference between $E_q{}'$ and U_v. P_e is the electromagnetic power of the synchronous generator, which can be regarded as the active output power when copper loss is ignored. P_v is the active power of the PV plant, P_s is the sum of the active power of the synchronous generator and the PV plant. X_1 is the sum of the transient reactance of the synchronous generator and the line reactance. In addition, X_2 is the line reactance on the side of the infinite-bus system.

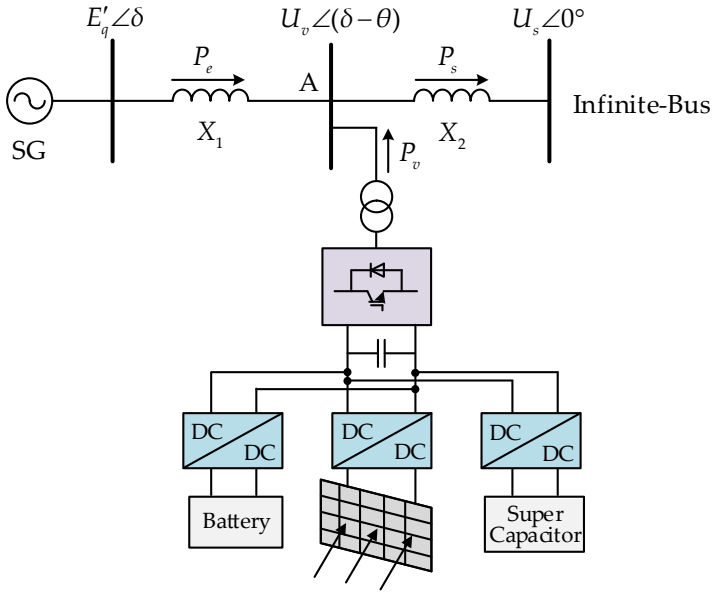

Figure 1. Structure of single-machine infinite-bus system for a PV plant.

2.1. Modeling of the SG

The rotor equations of the classical second-order model of the SG are shown in Equation (1).

$$\begin{cases} H\frac{d\omega}{dt} = P_m - P_e - D(\omega - 1) \\ \frac{d\delta}{dt} = \omega - 1 \end{cases} \tag{1}$$

H is the inertia time constant of the SG, P_m is the mechanical power of the SG, D is the damping coefficient, and ω is the rotor angular velocity. Linearizing Equation (1) at the equilibrium point, the resulting equation is given by the following:

$$Hs^2\Delta\delta + Ds\Delta\delta + \Delta P_e = 0 \tag{2}$$

2.2. Damping Performance Analysis of a Single-Machine Infinite-Bus System for a PV Plant

According to the power angle characteristic, the electromagnetic power of the SG can be described as the following:

$$P_e = \frac{E'_q U_v \sin\theta}{X_1} \tag{3}$$

$$P_s = \frac{U_v U_s \sin(\delta - \theta)}{X_2} \tag{4}$$

The power balance relationship at node A in Figure 1 is shown in Equation (5).

$$P_e + P_v = P_s \tag{5}$$

Linearizing Equations (3)–(5) at the equilibrium point, the resulting equations are shown as follows:

$$\Delta P_e = \frac{E'_q U_{v0} \cos\theta_0}{X_1}\Delta\theta + \frac{E'_q \sin\theta_0}{X_1}\Delta U_v \tag{6}$$

$$\Delta P_s = \frac{U_{v0} U_s \cos(\delta_0 - \theta_0)}{X_2}(\Delta\delta - \Delta\theta) + \frac{U_s \sin(\delta_0 - \theta_0)}{X_2}\Delta U_v \tag{7}$$

$$\Delta P_e + \Delta P_v = \Delta P_s \tag{8}$$

Substituting Equation (7) into Equation (8), the resulting equation is as the following:

$$\Delta P_e + \Delta P_v = \frac{U_{v0}U_s\cos(\delta_0-\theta_0)}{X_2}(\Delta\delta-\Delta\theta) + \frac{U_s\sin(\delta_0-\theta_0)}{X_2}\Delta U_v \tag{9}$$

Furthermore, Equation (6) can also be expressed as

$$\Delta\theta = \frac{X_1}{E'_qU_{v0}\cos\theta_0}\Delta P_e - \frac{\sin\theta_0}{U_{v0}\cos\theta_0}\Delta U_v \tag{10}$$

Substituting Equation (10) into Equation (9), the resulting equation is as the following:

$$\Delta P_e = K_0\Delta\delta + K_1\Delta U_v - K_2\Delta P_v \tag{11}$$

where

$$\begin{cases} K_0 = \frac{E'_qU_{v0}\cos(\delta_0-\theta_0)\cos\theta_0}{X_2E'_q\cos\theta_0 + X_1U_s\cos(\delta_0-\theta_0)} \\ K_1 = \frac{E'_qU_s\cos(\delta_0-\theta_0)\sin\theta_0 + E'_qU_s\sin(\delta_0-\theta_0)\cos\theta_0}{X_2E'_q\cos\theta_0 + X_1U_s\cos(\delta_0-\theta_0)} \\ K_2 = \frac{X_2E'_q\cos\theta_0}{X_2E'_q\cos\theta_0 + X_1U_s\cos(\delta_0-\theta_0)} \end{cases}.$$

Analyzing Equation (11) by the torque method, it can be found that ΔP_e can be composed of three parts. The first part ($K_0\Delta\delta$) is called synchronous torque and is in phase with $\Delta\delta$, where K_0 is the synchronous torque coefficient. The second part ($K_1\Delta U_v$) is proportional to ΔU_v and the third part ($-K_2\Delta P_v$) is inversely proportional to ΔP_v. Consequently, when LFOs occur in the system, the electromagnetic power of the SG can be adjusted through both the bus voltage of the grid-connection point and the active power output of the PV plant. The second and third parts are called damping torque, and the damping performance of the system depends on their phase relationship with $\Delta\omega$. Therefore, it is necessary to propose an effective additional damping control for the PV inverter to suppress LFOs.

3. ADC for the PV Inverter

3.1. Basic Principle of ADC for the PV Inverter

During the LFOs, the rotor angular velocity (ω) of SG swings up and down at the steady-state operating point (ω_0), and the schematic of rotor speed is shown in Figure 2.

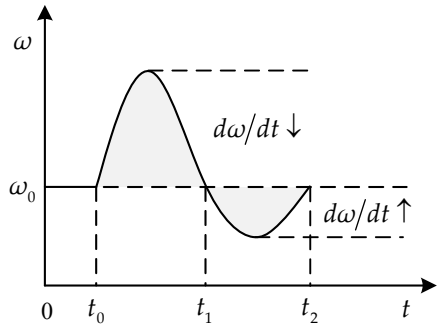

Figure 2. Schematic of rotor speed during the LFOs.

When ω is in the upper half-cycle of the oscillation ($\omega_0 < \omega$), $d\omega/dt$ should be reduced in order to quickly return to the steady-state operating point. According to Equation (1), since P_m is constant, P_e can be increased to reduce $d\omega/dt$. Conversely, when ω is in the lower half cycle of the oscillation ($\omega_0 > \omega$), P_e can be reduced to increase $d\omega/dt$. Based on the analysis of Equation (11) in Section 2.2, the expected relationships between ΔU_v, ΔP_v and ΔP_e are shown in the following table.

As can be seen from Table 1, the optimal damping performance of the system depends on whether both active and reactive damping play a positive damping role, which

requires that ΔU_v should be in the same phase with $\Delta\omega$ and ΔP_v should be in opposite phase with $\Delta\omega$.

Table 1. The expected relationships between ΔU_v, ΔP_v and ΔP_e.

Rotor Angular Velocity	Change Rate of w	Electromagnetic Power	Bus Voltage of Node A	Active Power Output
$\Delta\omega = \omega_0 - \omega < 0$	$d\omega/dt\downarrow$	$P_e\uparrow$, $\Delta P_e < 0$	$U_v\uparrow$, $\Delta U_v < 0$	$P_v\downarrow$, $\Delta P_v > 0$
$\Delta\omega = \omega_0 - \omega > 0$	$d\omega/dt\uparrow$	$P_e\downarrow$, $\Delta P_e > 0$	$U_v\downarrow$, $\Delta U_v > 0$	$P_v\uparrow$, $\Delta P_v < 0$

3.2. Additional Damping Controller

In order to suppress LFOs, this paper proposed the incorporation of an active additional damping controller into the PV inverter. The additional damping controller can be considered as a common structure of PSS, which is widely used due to its simple structure and principles. The local frequency deviation ($\Delta\omega$) is used as the input signal of the controller, and then the DC voltage reference of the PV inverter is obtained through the amplifier, the band-pass filter, the phase compensator and the amplitude-limiting link. The structure of the additional damping controller is shown in Figure 3.

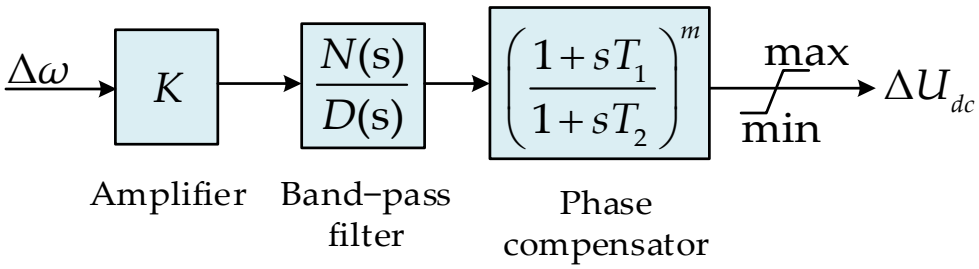

Figure 3. Block diagram of additional damping controller.

Amplifier: The gain coefficient (K) directly affects the damping performance of the additional damping controller. And the value of K is constrained by some conditions. The capacity of the energy storage device needs to be considered in active additional damping control, as does the margin of PV output and the allowed fluctuation range of the DC bus voltage. Conversely, the allowed fluctuation range of the AC bus voltage needs to be considered in reactive additional damping control.

Band-pass filter: Butterworth filter is used to attenuate DC and high-frequency components, only allowing the low-frequency components to pass.

Phase compensator: The angle to be compensated is the phase shift of the transfer function of the frequency measurement link and band-pass filtering link at the low-frequency oscillation point f_i. The phase compensator ensures that the additional damping controller can provide positive damping. The time constants T_1 and T_2 are given by Equation (12), θ is the angle to be compensated, and it is worth noting that the angle of compensation for each phase compensation link does not exceed 60°.

$$\begin{cases} a = \frac{T_1}{T_2} = \frac{1+\sin\theta}{1-\sin\theta} \\ T_1 = \frac{\sqrt{a}}{2\pi f_i}, T_2 = \frac{T_1}{a} \end{cases} \tag{12}$$

3.3. Small-Signal Modeling and Analysis of ADC for the PV Inverter

When the PV inverter adopts traditional control strategy, the following equations can be obtained.

$$\Delta P_v = 0, \Delta U_v = 0 \tag{13}$$

Substituting Equation (13) into Equation (11), the resulting equation is as follows:

$$\Delta P_e = K_0 \Delta\delta \tag{14}$$

Substituting Equation (14) into Equation (2), the resulting equation is as follows:

$$Hs^2\Delta\delta + Ds\Delta\delta + K_0\Delta\delta = 0 \tag{15}$$

From the above equation, it can be seen that the damping factor of the system is not changed. In other words, the PV plant fails to enhance the damping performance of the system.

When an additional damping controller is added to the active control link of PV inverter, the damping performance of the system will be enhanced. The block diagram of additional damping control is shown in Figure 4, where K_ω is the gain coefficient of additional damping controller.

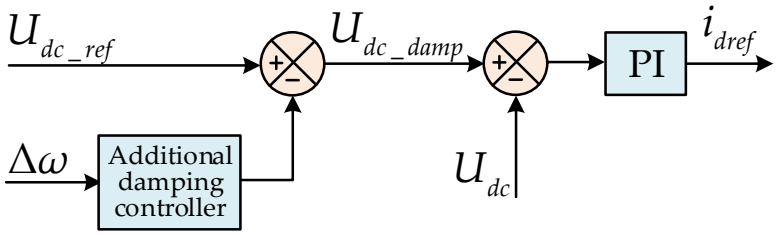

Figure 4. Block diagram of ADC.

It can be seen from Figure 4 that:

$$U_{dc\_damp} = U_{dc\_ref} - K_\omega \Delta\omega \tag{16}$$

where U_{dc_damp} is the new DC bus voltage reference. According to the decoupling characteristics of active power and reactive power, ΔU_v caused by active power is tiny which can be ignored. So, the following equations are obtained.

$$\begin{cases} U_{dc\_ref} - U_{dc} = \Delta U_{dc} = K_\omega \Delta\omega \\ U_{v\_ref} - U_v = \Delta U_v = 0 \end{cases} \tag{17}$$

The power stored in the DC capacitor is:

$$P_{dc} = \frac{1}{2} C_{dc} U_{dc}^2 \tag{18}$$

Linearizing Equation (18) at the equilibrium point, the resulting equation is given by the following:

$$\Delta P_{dc} = C_{dc} U_{dc0} \Delta U_{dc} = A\Delta U_{dc} \tag{19}$$

where C_{dc} is the DC side capacitance value, U_{dc0} is the DC bus voltage at steady state, $A = C_{dc}\ U_{dc0}$, in the case of ignoring the loss of PV inverter, ΔP_v and ΔP_{dc} are the same in size but opposite in direction. Therefore, ΔP_v can be expressed as

$$\Delta P_v = -\Delta P_{dc} = -AK_\omega \Delta\omega \tag{20}$$

Substituting Equations (17) and (20) into Equation (11), the resulting equation is as follows:

$$\Delta P_e = K_0 \Delta\delta + K_2 AK_\omega \Delta\omega \tag{21}$$

Substituting Equation (21) into Equation (2), the resulting equation is as the following:

$$Hs^2\Delta\delta + (D + K_2 AK_\omega)s\Delta\delta + K_0\Delta\delta = 0 \tag{22}$$

From Equation (22), the new damping coefficient of the system is

$$D' = D + K_2 A K_\omega \tag{23}$$

When $K_\omega > 0$, $D' > D$ due to A, $K_2 > 0$. It is effectively proved that the active additional damping control for the PV inverter can increase the damping coefficient of the system and enhance the ability to suppress LFOs.

4. Dynamic Power Compensation Control for HESS

4.1. HESS

For the PV plant without energy storage device, the damping performance is limited by the following three problems:

1. According to Equation (23), the damping effect is enhanced with the increase in K_ω. However, according to Equation (16), the deviation of the new reference value of DC bus voltage from the original reference value increases as K_ω increases. So the allowed fluctuation range of the reference value of DC bus voltage should be considered when setting the value of K_ω;
2. When the PV works at the maximum power point, the PV plant can only damp the upper half wave of the LFOs, which is because the PV inverter cannot increase the output power but only decrease it;
3. When the PV does not work at the maximum power point, the PV plant can damp the full wave of the LFOs, which is because the PV inverter can increase and decrease the output power. Additionally, the damping performance depends on the magnitude of power that the PV can adjust. Inevitably, a large amount of solar energy will be wasted.

Accordingly, configuring energy storage devices for PV plants is undoubtedly an effective solution to the above problems.

At the moment of LFOs or drastic changes in the external environment, the system suffers a short-term shock. At this time, the power to be compensated by the energy storage system is composed of high-frequency components and low-frequency components. Due to the battery having the characteristics of low power density and slow charging and discharging, it does not meet the requirements of charging and discharging with high power and fast speed. If only battery is used for power compensation, not only is the compensation effect not satisfactory, but also the service life of battery will be shortened. The super capacitor has the characteristics of high power density and fast charging and discharging, which can be used as a supplement to the energy storage system. A hybrid energy storage system composed of battery and super capacitor can better complete various power compensation tasks, and its equivalent mathematical model for hybrid energy storage can use the model proposed in [20].

4.2. ADC-Based DPCC

It is shown in Figure 1, the battery and the super capacitor are, respectively, connected to the DC bus through the Buck/Boost bidirectional converter. If the energy loss of the inverter is ignored, the power flow relationships of the PV plant are shown in Figure 5. Where P_{v_ref} is the active power reference value when the inverter does not add ADC. P_{v_damp} is the active power reference value when the inverter adds ADC. P_{sto_ref} is the active power reference value of the HESS. P_{pv} is the output power of the PV arrays; ΔP_v is the damping power provided by the HESS. ΔP_{pv} is the output power fluctuation of the PV array. P_{bat_ref} is the output power reference value of the battery. P_{sc_ref} is the output power reference value of the super capacitor.

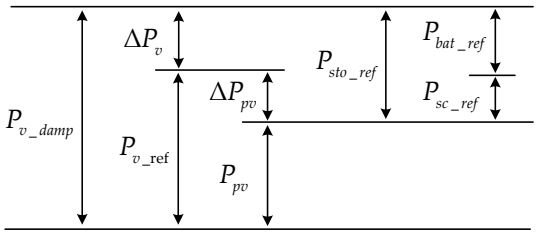

Figure 5. Power distribution diagram of the PV plant.

Additionally, they should also satisfy the following equations.

$$P_{v\_ref} = P_{pv} + \Delta P_{pv} \tag{24}$$

$$P_{v\_damp} = P_{v\_ref} + \Delta P_v \tag{25}$$

$$\begin{aligned} P_{sto\_ref} &= \Delta P_{pv} + \Delta P_v \\ &= P_{bat\_ref} + P_{sc\_ref} \end{aligned} \tag{26}$$

$$P_{bat\_ref} = P_{sto\_ref} \frac{1}{1 + sT} \tag{27}$$

$$P_{sc\_ref} = P_{sto\_ref} - P_{bat\_ref} \tag{28}$$

$1/(1 + sT)$ is the low-pass filter link and T is time constant.

The HESS has two power compensation goals: one is to compensate the output power of the PV arrays, and the other is to compensate the damping power required by ADC. In order for ΔP_v to be in opposite phase with $\Delta\omega$, the compensation power provided by the HESS should also be in opposite phase with $\Delta\omega$. Therefore, this paper proposed a DPCC based on ADC for HESS, where K is equal to AK_ω. Since both DPCC and ADC use $\Delta\omega$ as the input signal, it ensures that the compensation power provided by the HESS is in phase with the damping power required by the inverter. The block diagram of proposed ACDC, combining the ADC for the inverter with the DPCC for the HESS, is shown in Figure 6.

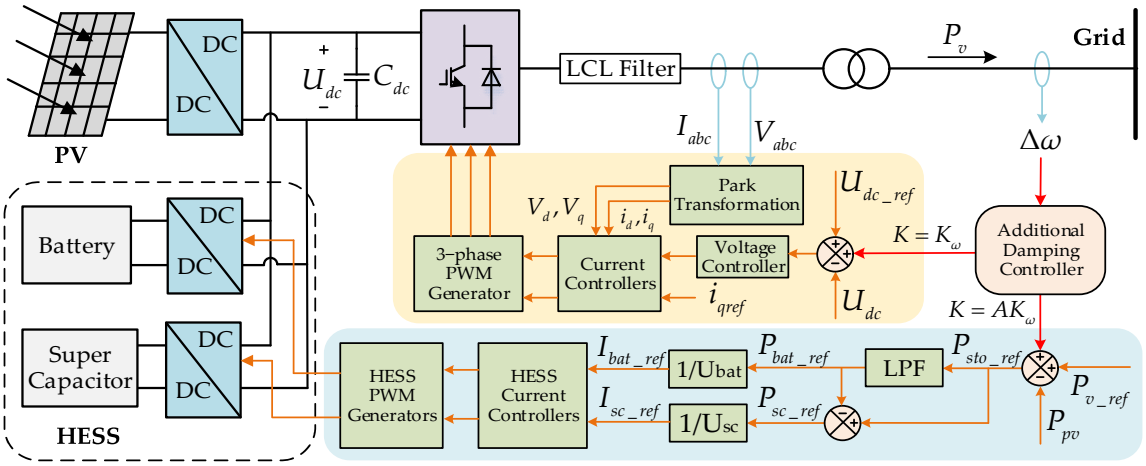

Figure 6. The block diagram of ACDC.

When the system does not generate LFOs, the HESS only compensates the power fluctuation of the PV arrays (ΔP_{pv}), and the power reference value of the HESS is given by Equation (29). When the LFOs occurs in the system, the HESS also needs to compensate the damping power required by the inverter (ΔP_v), and the power reference value of the HESS is given by Equation (30) at this time.

$$P_{sto\_ref} = P_{v\_ref} - P_{pv} \tag{29}$$

$$P_{sto\_ref} = P_{v\_ref} - P_{pv} + AK_{\omega}\Delta\omega \tag{30}$$

P_{sto_ref} is divided into P_{bat_ref} and P_{sc_ref} by the Butterworth low-pass filter, where P_{bat_ref} is the low-frequency components and P_{sc_ref} represents the high-frequency components. According to the energy complementary characteristics of the battery and super capacitor, they can respond quickly to power commands. HESS can effectively suppress the power fluctuation, improve power quality, and enhance the reliability and stability of the system.

5. Simulation Verification

In order to verify the effectiveness of the proposed damping control strategy in this paper, a simulation model of a three-machine nine-node system with a PV plant is built in PSCAD/EMTDC. At 8 s, a three-phase fault lasting 0.1 s will occur at bus 8, at which time there is an obvious LFO in the system.

The simulation topology is shown in Figure 7, and the ratings of the main parameters of the system are given in Table 2. U_{dc} is the DC bus voltage of the PV plant, P_{pv} is the output power of a PV array, P_{vsc} is the output power of a inverter (ignoring power loss), *Scale* is the number of PV arrays, and P_v is the output power of the PV plant.

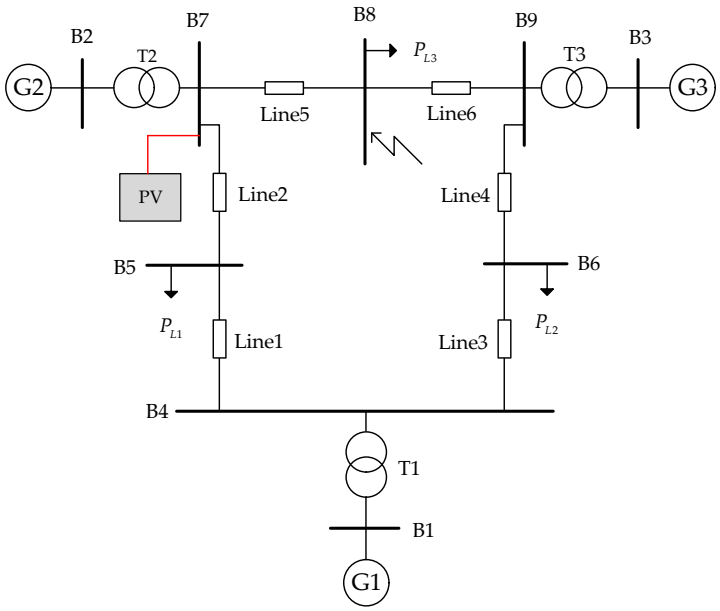

Figure 7. Topology of three-machine nine-node system with a PV plant.

Table 2. Ratings of the main parameters of the system.

Parameters	Value	Parameters	Value
B1	16.5 kV	U_{dc}	1 kV
B2	18 kV	P_{pv},P_{vsc}	0.34 MW
B3	13.8 kV	*Scale*	200
B4–B9	230 kV	P_v	68 MW
P_{L1}	125 MW + j50 Mvar	Irradiation	1200 W/m^2
P_{L2}	90 MW + j30 Mvar	Temperature	28 °C
P_{L3}	100 MW + j35 Mvar	Frequency	50 Hz

5.1. DPCC for HESS

Figure 8a shows that the active power output of a PV array has a variation of about 0.06 MW as the irradiation intensity decreases from 1200 W/m^2 to 1000 W/m^2 at 5 s and returns to 1200 W/m^2 at 15 s. According to Section 4.2, whether the damping power can be compensated quickly will directly influence the effect on suppressing the LFOs. It can be seen from Figure 8b that DPCC for HESS can quickly compensate the fluctuating power of

PV output and the damping power required by the inverter. P_{sto} is the output power of HESS and $DeltaP_v + DeltaP_{pv}$ is the compensation power required by the system. Figure 8c shows the power sharing link of the HESS, where P_{storef}, P_{scref} and P_{batref} are the power reference values for the HESS, super capacitor, and battery, respectively. It can be seen that the super capacitor is responsible for compensating high-frequency power, while the battery is responsible for compensating low-frequency power and providing long-term power support.

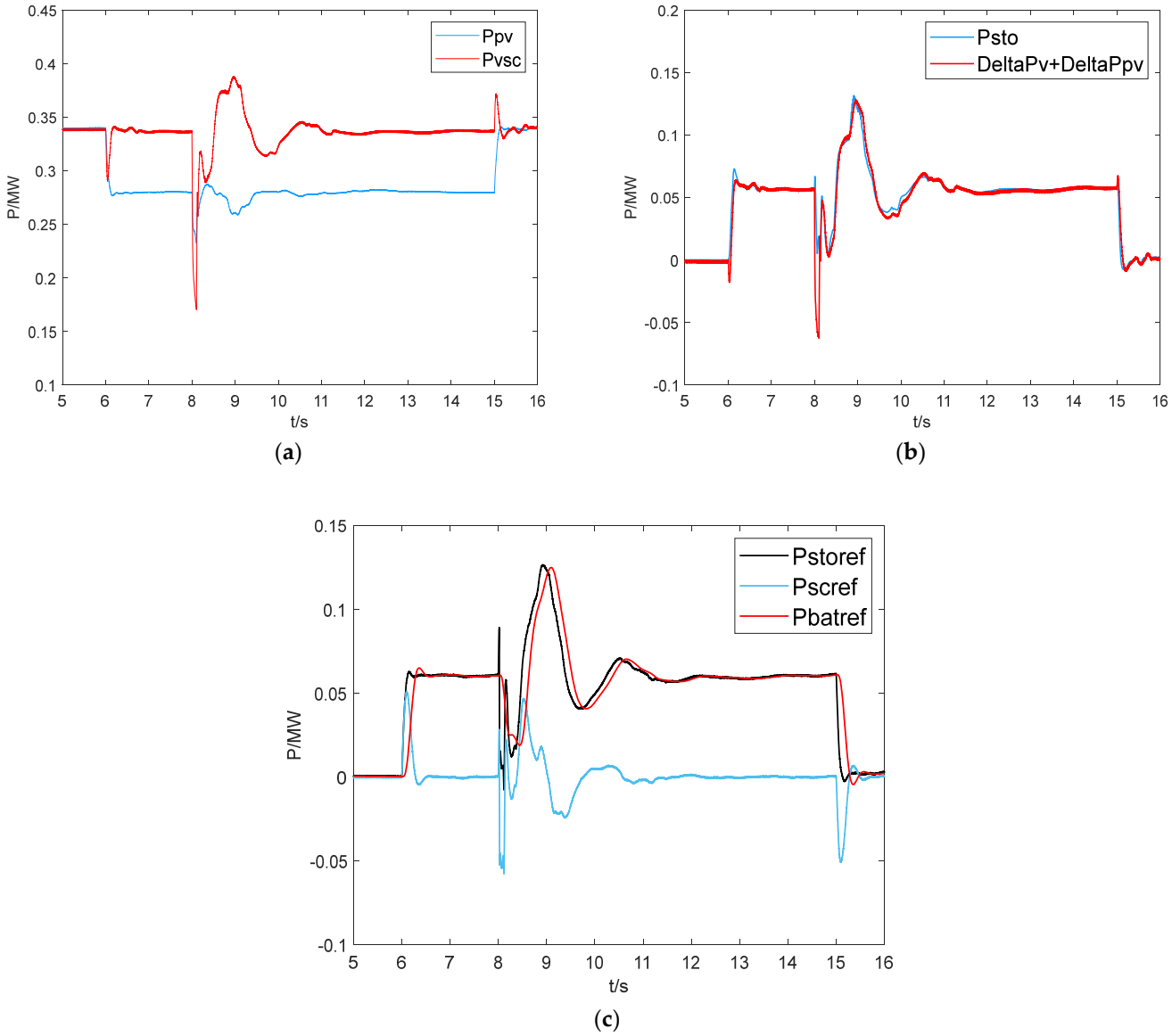

Figure 8. The power compensation effect of the HESS: (**a**) Active power output of a single PV array and inverter; (**b**) Dynamic power compensation for HESS; (**c**) Power sharing for the HESS.

5.2. ACDC Combining ADC with DPCC

This paper lists the following four damping control modes for the PV plant and compares their suppression effects on LFOs.

- NDC: The inverter adopts a traditional control strategy. The PV plant is not configured with HESS and works at the maximum power point;
- ADC 1: ADC is incorporated into the traditional control strategy of the inverter. The PV plant is not configured with HESS and works at the maximum power point;

- ADC 2: ADC is incorporated into the traditional control strategy of the inverter. The PV plant is not configured with HESS and works at the non-maximum power point;
- ACDC: ADC is incorporated into the traditional control strategy of the inverter. The PV plant is configured with HESS which adopts DPCC and works at the maximum power point.

It can be seen from Figure 9 that the phase deviation between the output power of PV plant and the frequency cannot always be 180° in mode ADC 1. Although the low-frequency amplitude gradually decreases, there is no significant effect on shortening the oscillation period. However, in modes ADC 2 and ACDC, the output power is always phase opposite to the frequency, which makes the low-frequency amplitude decrease rapidly and the oscillation period shorten significantly. In particular, the proposed control not only suppresses the LFO well, but it also enables the PV plant to always maintain the maximum output power and avoid the waste of solar energy.

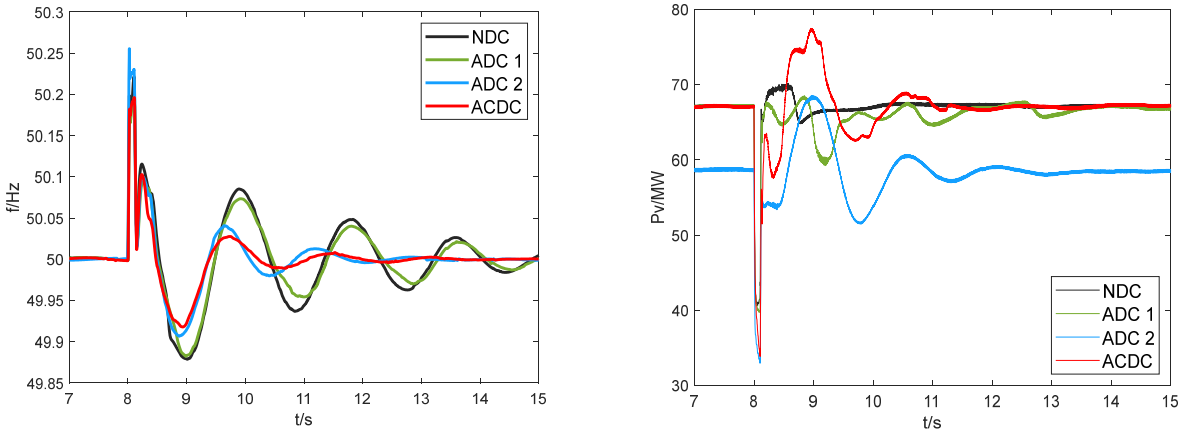

(**a**) (**b**)

Figure 9. Comparison of the suppression effects of four control modes: (**a**) Tie-line frequency of the PV plant; (**b**) Active power injected into the system of the PV plant.

As can be seen in Figure 10, if there is no power compensation source, the PV inverter with only ADC will cause dramatic and long-term fluctuations in the DC bus voltage. In mode ACDC, the DC bus voltage is within a small fluctuation range and can restore to stability quickly.

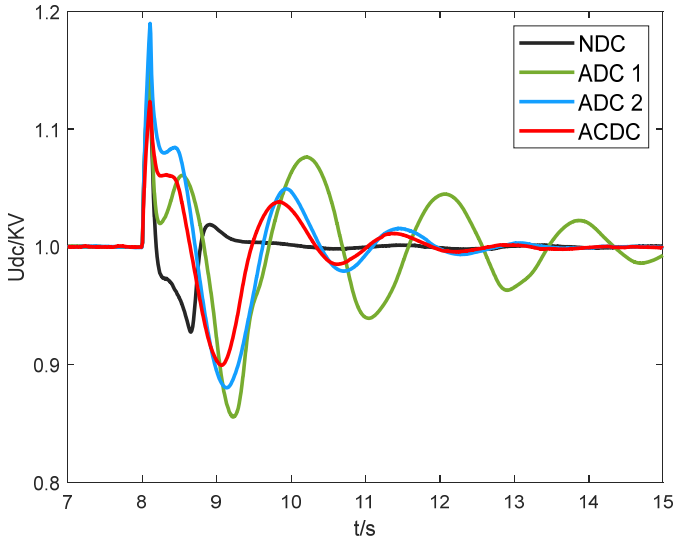

Figure 10. DC bus voltage of the PV plant.

6. Conclusions

Due to the increased proportion of PV power generation, the LFOs are prone to occur during power system failures. To reduce the risk of LFOs to the power system, PV plants should suppress the LFOs through a damping control strategy. In this paper, an ACDC which combines ADC for the inverter and ADC-based DPCC for the HESS was proposed to suppress the LFOs. The following conclusions are drawn from the whole analysis:

- ADC is demonstrated to improve the damping performance of the system by the analysis of torque method and the small signal model;
- The damping performance of ADC depends on the compensation power. The ACDC not only obviously enhances the damping performance of the PV plant during LFOs but also maintains the stability of the PV output and avoids the waste of solar energy.

Author Contributions: Conceptualization, K.D., W.X. and X.Y.; methodology, K.D. and X.Y.; software, K.D. and X.Y.; validation, K.D., W.X. and Y.C.; formal analysis, X.Y. and W.X.; investigation, Q.F., Y.X. and Y.C.; resources, X.Y.; data curation, K.D. and D.G.; writing—original draft preparation, K.D.; writing—review and editing, X.Y.; visualization, W.X.; supervision, H.Z.; project administration, X.Y. and H.Z.; funding acquisition, X.Y. and H.Z. All authors have read and agreed to the published version of the manuscript.

Funding: This work was supported by National Natural Science Foundation of China (NSFC) (No. 52067004, No. 52167007), Guizhou Provincial Science and Technology Projects (ZK [2022] General 154; [2022] General 012).

Institutional Review Board Statement: Not applicable.

Informed Consent Statement: Not applicable.

Data Availability Statement: Not applicable.

Acknowledgments: This work was supported by the Distribution Network Energy Conservation and Loss Reduction Research Group of the School of Electrical Engineering of Guizhou University and the Electric Power Research Institute of Guizhou Power Grid Co., Ltd.

Conflicts of Interest: The authors declare no conflict of interest.

References

1. BNEF. New Energy Outlook. Available online: https://www.power-technology.com/news/bloomberg-new-energy-outlook-2019-2/ (accessed on 11 April 2021).
2. International Energy Agency. *Renewables 2021—Analysis and Forecast to 2026*; International Energy Agency: Paris, France, 2021.
3. Moghassemi, A.; Padmanaban, S.; Ramachandaramurthy, V.K.; Mitolo, M.; Benbouzid, M. A novel solar photovoltaic fed TransZSI-DVR for power quality improvement of grid-connected PV systems. *IEEE Access* **2021**, *9*, 7263–7279. [CrossRef]
4. Quintero, J.; Vittal, V.; Heydt, G.T.; Zhang, H. The impact of increased penetration of converter control-based generators on power system modes of oscillation. *IEEE Trans. Power Syst.* **2014**, *29*, 2248–2256. [CrossRef]
5. Zhu, F.; Zhao, H.; Liu, Z.; Kou, H. The Influence of Large Power Grid Interconnected on Power System Dynamic Stability. *Proc. CSEE* **2007**, *27*, 1–7.
6. Shah, R.; Mithulananthan, N. A comparison of ultracapacitor, BESS and shunt capacitor on oscillation damping of power system with large-scale PV plants. In Proceedings of the AUPEC 2011, Hawaii, HI, USA, 11 November 2011; pp. 1–6.
7. Lei, X.; Lerch, E.; Povh, D. Optimization and coordination of damping controls for improving system dynamic performance. *IEEE Trans. Power Syst.* **2001**, *16*, 473–480.
8. Kahouli, O.; Jebali, M.; Alshammari, B.; Abdallah, H.H. PSS design for damping low frequency oscillations in a multi-machine power system with penetration of renewable power generations. *IET Renew. Power Gener.* **2019**, *13*, 116–127. [CrossRef]
9. Gurrala, G.; Sen, I. Power system stabilizers design for interconnected power systems. *IEEE Trans. Power Syst.* **2010**, *25*, 1042–1051. [CrossRef]
10. Lam, D.M.; Yee, H. A study of frequency responses of generator electrical torques for power system stabilizer design. *IEEE Trans Power Syst.* **1998**, *13*, 1136–1142. [CrossRef]
11. Zhang, X.; Lu, C.; Liu, S.; Wang, X. A review on wide-area damping control to restrain inter-area low frequency oscillation for large-scale power systems with increasing renewable generation. *Renew. Sustain. Energy Rev.* **2016**, *57*, 45–58. [CrossRef]
12. Suo, J.; Hu, Z.; Liu, Y.; Zhang, Z. Influence of Large-Scale Photovoltaic System Integration on Damping Characteristics of Interconnected Grid and Damping Control. *J. Xi'an Jiaotong Univ.* **2015**, *49*, 99–105. [CrossRef]

13. Xiong, H.; Wang, Z.; Shang, L.; Dong, X. Design and Analysis of the Damping Injection Control of Renewable Power Plants for Low Frequency Oscillation Mitigation of Power System. *Power Syst. Technol.* **2022**, *46*, 2690–2700. [CrossRef]
14. Chaiyatham, T.; Ngamroo, I. Improvement of power system transient stability by PV farm with fuzzy gain scheduling of PID controller. *IEEE Syst. J.* **2017**, *11*, 1684–1691. [CrossRef]
15. Du, W.; Wang, H.; Xiao, L.Y. Power system small-signal stability as affected by grid-connected photovoltaic generation. *Eur. Trans. Electr. Power* **2012**, *22*, 688–703. [CrossRef]
16. Prasertwong, K.; Mithulananthan, N.; Thakur, D. Understanding Low-Frequency Oscillation in Power Systems. *Int. J. Electr. Eng. Educ.* **2010**, *47*, 248–262. [CrossRef]
17. Shah, R.; Mithulananthan, N.; Lee, K.Y. Large-Scale PV Plant With a Robust Controller Considering Power Oscillation Damping. *IEEE Trans. Energy Convers.* **2013**, *28*, 106–116. [CrossRef]
18. Saadatmand, M.; Gharehpetian, G.B.; Moghassemi, A.; Guerrero, J.M.; Siano, P.; Alhelou, H.H. Damping of Low-Frequency Oscillations in Power Systems by Large-Scale PV Farms: A Comprehensive Review of Control Methods. *IEEE Access* **2021**, *9*, 72183–72206. [CrossRef]
19. Saadatmand, M.; Mozafari, B.; Gharehpetian, G.B.; Soleymani, S. Optimal damping controller design for large-scale PV farms to damp the low-frequency oscillation. *Int. J. Renew. Energy Res.* **2019**, *9*, 1672–1680.
20. Mohamed, M.M.; El Zoghby, H.M.; Sharaf, S.M.; Mosa, M.A. Optimal virtual synchronous generator control of battery/supercapacitor hybrid energy storage system for frequency response enhancement of photovoltaic/diesel microgrid. *J. Energy Storage* **2022**, *51*, 104317. [CrossRef]